Ovine Adipose Tissue Material Characterisation, Model Development and Validation

Patricia K. Thomas, Kyle Ondar, Philip J. Brown, F. Scott Gayzik

Abstract High-rate non-penetrating blunt injury (NPBI) occurs from an impact to the body without penetration, in which the thorax is a common site of impact, leading to injury. One of the major tissues that are known to absorb energy from NPBI is adipose tissue, but ovine adipose tissue has not been well documented in literature. Due to the loading rate dependencies of adipose tissue, this study utilises a three-parameter Maxwell viscoelastic model for characterisation. Four post-mortem samples from two donors were used for spherical indentation testing, where each was tested at each loading rate (0.2 mm/s, 2 mm/s, 20 mm/s, 200 mm/s). Statistical tests on the resulting shear moduli were conducted via a mixed model. The relaxed shear modulus was not influenced by the velocity ($p>0.05$); however, the instantaneous modulus at the lowest loading velocity was different from the others ($p<0.05$). After indentation testing, each sample was impacted at 4 m/s, 6 m/s, and 7 m/s to obtain data for validation. Due to the nature of experimental testing, impact angles ranging from 0° to 20° from the vertical were simulated *in silico*, successfully matching the range of experimental data traces. Force-time data traces were output and plotted against experimental dynamic data, validating the simulated tissue behaviour.

Keywords Adipose, blunt injury, finite element modeling, material characterisation, viscoelasticity.

I. INTRODUCTION

High-rate non-penetrating blunt injury (NPBI) is known to cause injury to any underlying organs. Injuries have been known to include lung contusions, broken ribs, bruising, as well as internal bleeding depending on where the impact occurred [1]. Ovine animal models have been established as viable surrogates for studying NPBIs due to similar lung physiology to humans. They are a common model for studying high-rate injuries and can be found in decades' worth of military experiments [2-4]. With the large amount of experimental data available, finite element (FE) models of ovine are being developed to study injury risk to various organs from NPBIs, but they require more specific material inputs for the tissues impacted [5].

While the first tissue impacted in the high-rate NPBI environment is the skin, immediately below it lies the adipose tissue, which has been established in the literature as an energy-absorbing structure [6-7]. The presence of adipose tissue superficially coupled with its energy-absorbing qualities suggests that it influences the injury risk to the organs deep to it. This makes it important to understand adipose tissue behaviours. To understand its behaviour, it is important to understand its structure. Adipose tissue is known to be composed of connective tissue with adipocytes and triglycerides [8]. Comley *et al*. found that the triglycerides individually have a viscosity of 36.8 mPas, which is comparable to cream or vegetable oil [9]. Between 60% and 80% of adipose tissue by mass is made up of lipids, like triglycerides, and an additional 5–30% by mass is made up of water [8]. Therefore, it is imperative to properly account for the large amount of fluid in the tissue when modelling it, particularly in situations such as high-velocity NPBI environments.

One material model that is used for modelling soft tissues is a viscoelastic material model. Due to its large fluid content, adipose tissue is considered to be viscoelastic [8][10-18]. Indentation tests can be used to measure viscoelasticity through stress-relaxation, which is important to understand material behaviour. Within fibrous materials, fluid flow patterns and fiber orientation affect viscoelastic behaviour [19]. In biological materials, how the extracellular fluid flows through the extracellular matrix determines the viscoelastic parameters, which can be experimentally determined. Water makes up anywhere between 55% and 75% of humans, depending on age,

F. S. Gayzik (e-mail: sgayzik@wakehealth.edu; tel: +1(336)716-6643) is a Professor, P. K. Thomas is a PhD student and P. J. Brown is an Associate Professor in the Department of Biomedical Engineering at Wake Forest University in Winston-Salem, NC, USA. K. Ondar was a research engineer at Wake Forest University at the time of work completion and is now a biomedical engineer at the Walter Reed Army Institute of Research in Silver Spring, Maryland, USA.

making it important to understand how it affects material behaviour [20]. Viscoelastic material models account for this movement, which makes it imperative to broadly account for it in FE models.

The use of a viscoelastic model, in this case, a Maxwell viscoelastic model, theoretically accounts for tissue relaxation that occurs during the tissue-loading phase in experiments with a ramp correction factor (Eq. 1) when calculating material coefficients [21-24].

$$RCF_k = \frac{\tau_k}{t_R}[e^{(t_R/\tau_K)} - 1] \quad (1)$$

This would allow it to potentially be of use at different rates, particularly in FE modelling. To calculate each RCF_k, the time constants (τ_K) and the ramp time (t_R) are calculated using the displacement data. The final material coefficients can be calculated using the results of a stress-relaxation experiment, where the specimen is loaded to a specific displacement and the resulting force is measured for the duration of the experiment [21-22][24-27]. Similar methods have been used to evaluate tissues, including bone, lung, cartilage, and adipose tissue [21-22][24][28-29]. When using a spherical indenter head these experiments are non-damaging, therefore the same samples can be used for multiple experiments [21][24]. While Eq. (1) is an equation that accounts for any relaxation that occurs prior to peak depth, it has been primarily used for stiffer materials, such as bone and cartilage [22][24][30]. One goal of this study is to determine at what strain rate a linear viscoelastic assumption is appropriate, as at lower loading rates a non-linear viscoelastic model may be more appropriate. Overall, the goal of this study is to characterise ovine adipose tissue and then validate the resulting material model *in silico* for applications in high-velocity applications, such as NPBI.

II. METHODS

Sample Procurement

Ovine adipose tissue specimens were obtained as refuse tissue from a concurrent study utilising ovine subjects (#A22-103). The adipose tissue collected from the animals was not subjected to any surgical, chemical, or physiological interactions prior to extraction. The study followed all protocols set forth by the Wake Forest University Health Sciences Animal Care and Use Committee. A sample was collected from the flanks of each animal (N=2), for a total of four separate adipose samples, all on the same day. Both animal donors were female, between 7-8 years of age. Both had been severely obese, with some mass loss prior to sacrifice. Samples ranged in thickness from 2 cm to 4 cm, in width from 9 cm to 18 cm, and in length from 15 cm to 20 cm. After collection, each sample was wrapped in saline-soaked gauze and frozen, as freezing adipose tissue had been shown to not affect the material properties [11]. Samples were thawed two days prior to testing in the refrigerator, and at room temperature the morning of testing. All samples were tested on the same day to prevent time frozen from having an effect. Prior to testing, adipose samples were hydrated with saline.

Indentation Tests

Spherical indentation tests were run at four different loading rates of 0.2 mm/s, 2 mm/s, 20 mm/s, and 200 mm/s for a total of 78 tests. The order of loading rate alternated on each day for each sample. An MTS hydraulic testing frame (MTS Systems, Eden Prairie, MN) was used to run these tests. The sample was placed on a specimen board to prevent lateral movements, as seen in Fig. 1. A Delrin® sphere with a 0.75 inch diameter was adapted to attach to the top-mounted 500 N load cell. The indenter indented each sample to a depth of 4 mm and held a constant displacement for 90s. Time, force, and displacement were recorded for material analysis. Each test was completed at a different location to follow Hertzian assumptions [21][23].

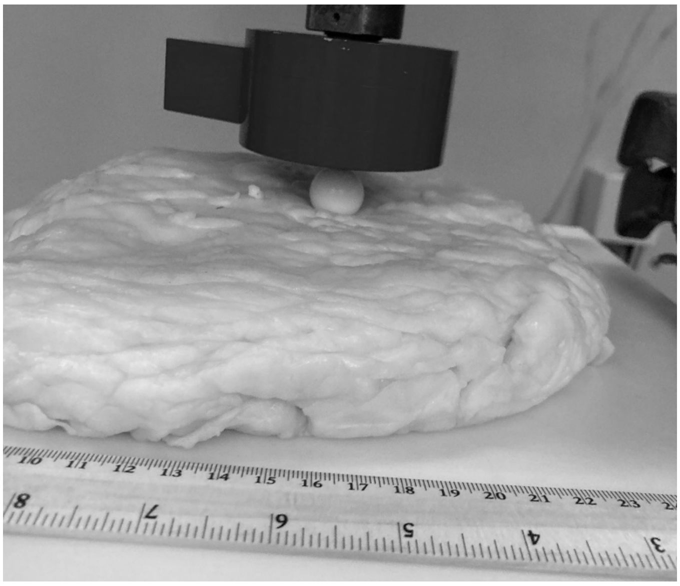

Fig. 1. Example spherical indentation test.

Due to the higher rate of loading, particularly with the 20 mm/s and 200 mm/s loading rates, inertial loading was corrected for prior to any data analysis. For consistency, the inertial loading calculation was done on every test, regardless of loading velocity. The velocity was calculated based on the displacement and time data, the time of impact was determined, and the acceleration was calculated from velocity. Since the mass of the indenter is known, the inertial loading can be calculated using Newton's second law. The inertial loading force was then subtracted from the total measured force, leaving the actual force for material analysis. The data were then filtered using a moving mean filter, and the time of contact through the end of the experiment was isolated (peak force until the end of the test) was fit to the viscoelastic material model. All this analysis was done using a custom code that utilises existing toolboxes in MATLAB 2022b (Mathworks, Natick MA).

Material Theory and Calculations

The shear modulus relaxation equation (Eq. 2) that is derived from the 3-parameter Maxwell viscoelastic material model:

$$G(t) = C_0 + \sum C_k e^{-t/\tau_k} \tag{2}$$

accounts for the loading rate using the RCF (Eq. 3) and ramp time (t_R), as seen in Eqs 2–5 [21-22][24]. This material model utilises the ramp time (t_R) and ramp correction factor (RCF), which is defined as the time from contact until the indenter reaches maximum depth (h), to account for any relaxation that occurs during the loading phase of an indentation test.

$$RCF_k = \frac{\tau_k}{t_R}\left[e^{(t_R/\tau_K)} - 1\right] \tag{3}$$

$$C_0 = \frac{B_0}{h_{max}^{3/2}(8\sqrt{R}/3)} \tag{4}$$

$$C_k = \frac{B_k}{(RCF_k)h_{max}^{3/2}(8\sqrt{R}/3)} \tag{5}$$

Each C_K is calculated using a curve fit to the experimental force-time data, which is seen in Eq. 6:

$$P(t) = B_0 + \sum B_k e^{-t/\tau_k} \tag{6}$$

P(t) is the force over time, and the constants B_k are force values. The time constants, τ_K, are also from this curve fit and are used in Eqs 2 and 3. The variable *h* is the maximum depth of a specific test and was calculated using each test's respective displacement data. The last variable, *R*, is the radius of the indenter tip, which is constant across all tests.

Based on the resulting C_K values, the instantaneous and relaxed shear moduli can be calculated (Eq. 7 and Eq. 8). These were calculated to compare to existing literature and for statistical analyses:

$$G_0 = \frac{C_0 + C_1 + C_2 + C_3}{2} \quad (7)$$

$$G_\infty = \frac{C_0}{2} \quad (8)$$

Indentation Statistical Analyses

The resulting instantaneous and relaxed shear moduli were each analysed to determine if the loading rate influenced the shear modulus. An ANOVA with post-hoc Tukey tests was run in MATLAB to determine if the loading rate and/or animal subject influenced each respective property ($\alpha = 0.05$). Post-hoc tests would assist in determining strain rate sensitivity.

eCCI Impact Tests

After all indentation tests were completed, electric cortical contusion impactor (eCCI) impacts were run on every sample. Impacts were completed using an eCCI (Custom Design & Fabrication Inc, Sandston VA) instrumented with a piezoelectric load cell (208C02, PCB Piezotronics, Depew NY), as seen in Fig. 2. Due to the large size of each sample, each sample had six impacts with two impacts at each velocity (4 m/s, 6 m/s, and 7 m/s). Every test, regardless of velocity, impacted the sample to a depth of 10 mm from the surface of the tissue. Impacts were completed at different locations from one another due to the damage that occurred during the impacts. Force data were collected over the duration of the impact for material validation to be completed. Peak forces were compared with a multivariate mixed model using JMP (SAS Institute, Cary NC).

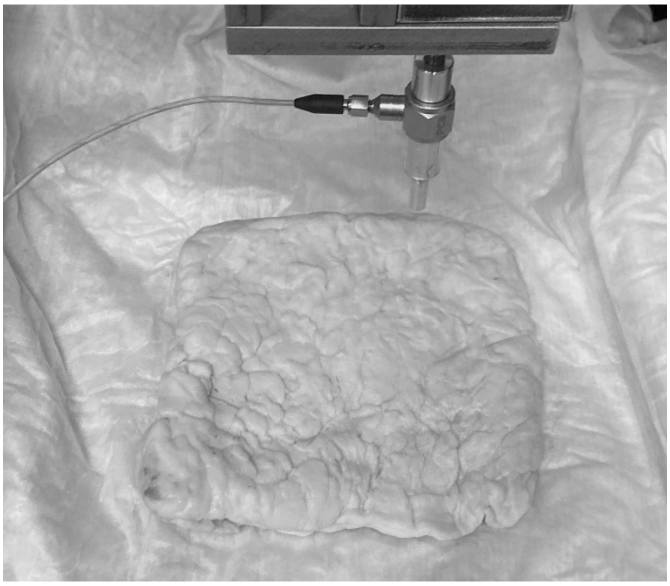

Fig. 2. Example eCCI set-up with adipose tissue.

eCCI Simulations

This simulation was set-up to include the adipose tissue block (66,240 hexahedral elements) and the impactor (525 hexahedral elements) in LS-DYNA (ANSYS, Canonsburg, PA). A *MAT_GENERAL_VISCOELASTIC material card was utilised with a set of parameters resulting from fitting the adipose tissue indentation data (Table I). The bottom of the adipose tissue was constrained to prevent lateral or vertical movement. The impactor loaded the tissue at a velocity of 4 m/s and to a depth of 10 mm to match experimental protocols. As indicated by the statistical analysis of the eCCI *ex vivo* impacts, no difference was found between loading rates, so only one impact velocity was simulated. No failure strains were input into the model due to the lack of available ovine-specific adipose failure data in literature. The velocity of the impactor was constant throughout the event.

TABLE I
ADIPOSE TISSUE MATERIAL INPUTS MEASURED PARAMETERS

Material Parameter	Units	Value
ρ	kg/mm^3	8.33E-07
K	GPa	5.68E-04
G_0	GPa	9.11E-06
G_1	GPa	6.59E-06
β_1	1/ms	1.72E-05
G_2	GPa	3.28E-06
β_2	1/ms	1.44E-05
G_3	GPa	3.89E-06
β_3	1/ms	9.56E-04

An additional three simulations were run to determine angle sensitivity due to the not perfectly flat nature of the adipose tissue surface, where the impactor was angled at 5°, 10° and 20° from the vertical axis. Resulting contact forces were filtered using a low pass J211 SAE 1000 filter. The resulting force-time trace was then plotted against corridors calculated using ArcGen for final validation [31].

III. RESULTS

Indentation

The loading velocity did not influence the relaxed shear modulus (p=0.214), but it was considered to have an effect on the instantaneous shear modulus (p=0.002), as seen in Fig. 3.

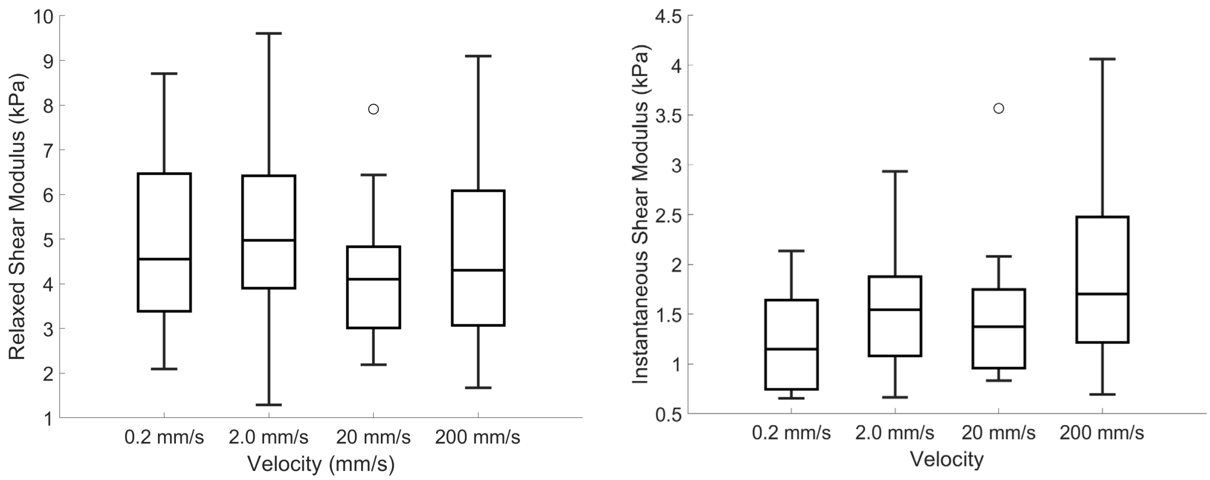

Fig. 3. (Left) Boxplot with relaxed shear modulus over each velocity. (Right) Boxplot with instantaneous shear modulus at each velocity.

However, for both moduli the animal subject that the tissue originated from did have an effect (p < 0.0001). The interaction between velocity and animal was not significant for either modulus. When specifically looking at the post-hoc comparisons of velocity, there were no differences between velocities for the relaxed modulus, showing that the velocity was properly accounted for within the shear modulus calculations. However, the case was not identical for the instantaneous modulus. The post-hoc comparisons showed that the group loaded at 0.2 mm/s was different from both 2 mm/s and 200 mm/s (p<0.05). The effect that animal had was very pronounced on both moduli, with p < 0.001 for both. This is visible visually as well for both moduli (Fig. 4).

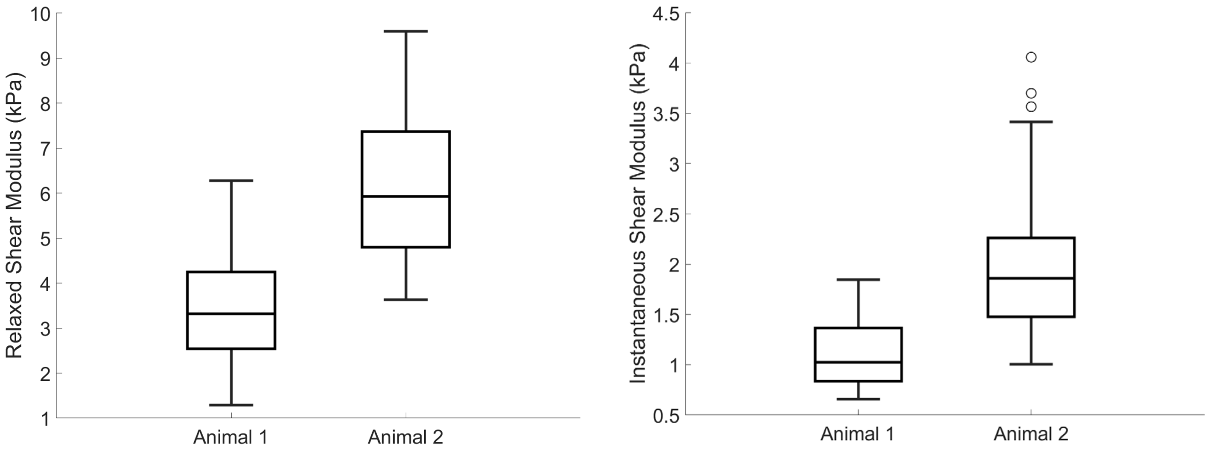

Fig. 4. (Left) Boxplot with relaxed shear modulus by animal. (Right) Boxplot with instantaneous shear modulus by animal.

eCCI

Peak forces from eCCI impacts were compared using a multivariate mixed model but were not found to be significant ($p > 0.05$). Differences were not detected at these velocities, likely due to the proximity of all three impact velocities, whereas the indentation loading velocities were separated by one to four orders of magnitude. Tissue failure was noted after each impact, as a crater matching the impacting anvil was visible. The resulting force-time data traces can be seen in Fig. 5.

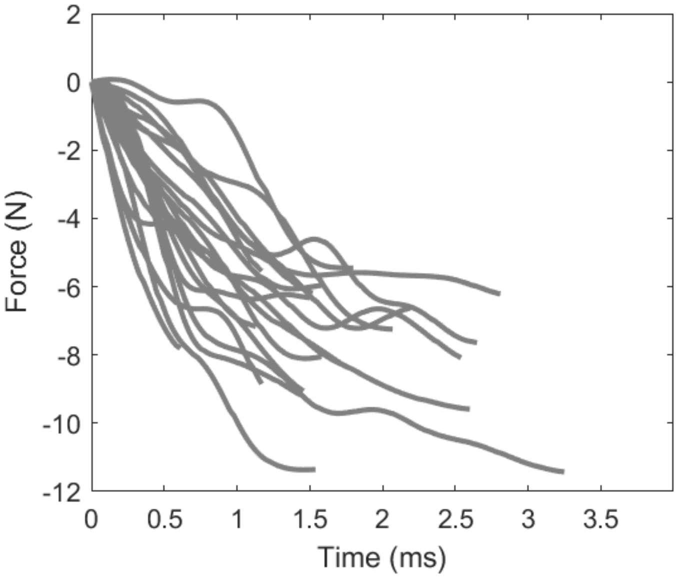

Fig. 5. All force-time data traces from eCCI impacts.

eCCI Simulations

Overall, the simulated force-time data traces match well with the experimental data. All four simulations were stable throughout the impact. As seen in Fig. 6, as the angle increased, the initial spike and oscillations in the force decreased. No failure or element erosion was used in these simulations, which may contribute to the initial overestimation of force during the more perpendicular impacts. Overall, the simulated force-time data traces match well with the experimental data corridors, particularly as the angle from the vertical increased to 20°. The sample, unlike the model, was not perfectly planar, which we believe helps explain the presence of the prominent spike in the simulated data at zero and five degrees.

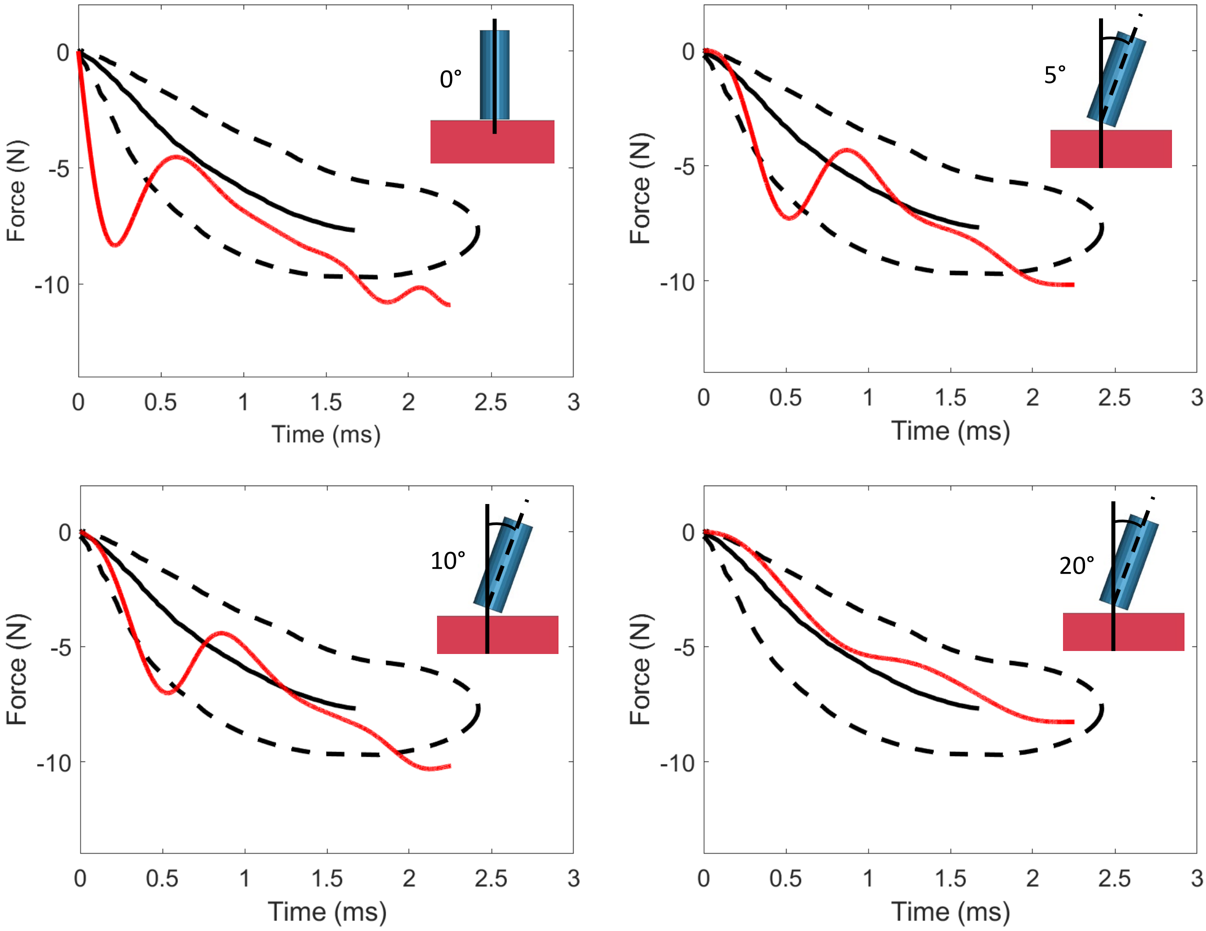

Fig. 6. (Top Left) 0° from vertical axis impact. (Top Right) 5° from vertical axis impact. (Bottom Left) 10° from vertical axis impact. (Bottom Right) 20° from vertical axis impact. Simulation data in red plotted against corridors developed from all experimental data using ArcGen [31].

IV. DISCUSSION

This study characterised and validated ovine adipose tissue properties. The characterisation occurred over a range of loading velocities to ensure sufficient accounting for loading that occurred prior to peak displacement. Dynamic testing was also completed for use in validation, where *in silico* force-time data traces were found to vary depending on the angle of impact, but generally matched experimental data.

This work, to the authors' knowledge, is the first to characterise ovine adipose tissue, as there is limited literature on the material properties of ovine tissue as a whole. Previous adipose tissue characterisation studies used porcine and human tissue [10][12-13][18][28][32]. One previous study [11] investigated the effects of freezing on human adipose tissue material properties and showed that the effects of freezing were not significant. Despite the high variability, the resulting shear moduli, both instantaneous and relaxed, are of a logical magnitude based on other types of adipose tissue tested throughout literature. Our mean instantaneous shear modulus is 15.71 ± 7.53 kPa, whereas the relaxed shear modulus is 4.75 ± 1.97 kPa. In [11], Sun *et al.* tested human adipose tissue using puncture indentation at a low rate (about 0.24 m/s) and calculated a 4 kPa shear modulus. The same study also tested porcine tissue at the same rate, calculating a shear modulus of 75 kPa [11]. In [10], Comley *et al*. tested porcine at a large range of strain rates to fit an Ogden rubber material model, and calculated shear moduli ranging from 0.4 kPa to 1112 kPa. For comparison purposes, we can estimate a strain rate using our data, where we assume ε is 1, and approximate the ramp time (t) using Eq. 9, where x is the depth (4 mm) and v is the loading rate (0.2 mm/s, 2 mm/s, 20 mm/s, or 200 mm/s):

$$t = \frac{x}{v} \tag{9}$$

The estimated strain rates are shown in Table II.

TABLE II
APPROXIMATED STRAIN RATES FOR EACH SPHERICAL INDENTATION LOADING VELOCITY

Loading Velocity (mm/s)	Strain Rate (ε/s)
0.2	0.05
2	0.5
20	5
200	50

This demonstrates that our data for ovine adipose tissue falls between human and porcine material properties, which are structurally different, with different proportions of different lipids [11]. The material model was characterized using the range of strain rates tested (Table 2), which constitutes a fairly large range, leading to the Generalized Maxwell model being considered acceptable for a range of applications. For comparison purposes, the impact tests using the eCCI using Equation 9 were loading the samples at strain rates between 400 – 700 ε/s.

Another notable study worth comparing to would be Gefen et al [33]. In their study, Gefen et al. investigated the viscoelasticity of ovine white adipose tissue. The tissue was freshly extracted from the gluteus muscles, a different region from what this study used, which was white adipose tissue superficial to the ribs. While both this study and Gefen et al. completed viscoelasticity studies, Gefen et al. used a confined compression test set-up with a cylindrical platen loading the sample, resulting in more macroscopic properties than our more localized testing set-up. Gefen et al. and this study used similar loading rates and depths for the boundary conditions. However, due to the different testing set-ups, a different set of data is calculated. Gefen et al. calculated the aggregate modulus over time, which was converted to Young's modulus over time, whereas we calculated the shear modulus over time. A limitation that Gefen et al. has is the assumed Poisson's ratio of 0.495 [33]. Our analysis does not require Poisson's ratio to calculate the shear modulus, simply the geometry of the test set-up. Gefen et al. had a mean calculated Young's modulus for their confined compression test of 860 Pa, whereas if we convert our shear modulus to Young's modulus using the same Poisson's ratio, we have a modulus two magnitudes higher at 46.97 kPa. It is not possible to compare the relaxed modulus values between the studies due to the different hold times used by each study, where their hold time was 240s, compared to our 90s hold.

While these values are in a similar range as other adipose tissues, there were assumptions made in these experiments, the largest of which is linear viscoelasticity. It was assumed that the loading rate is linearly correlated to the stress-relaxation curve during the loading time, when this may only be true above a specific strain rate or relaxation can be approximated as linear above a specific rate. This assumption is one reason that the instantaneous modulus was considered statistically different at the 0.2 mm/s loading rate and not at the other three loading rates. Comley *et al*. suspected that there is a strain rate sensitivity switch at a specific strain rate, whereby the tissue behaves stiffer after the switch. This was identified as roughly 10 ε/s based on their data when looking at the elastic modulus relaxation, whereas the data from this study suggests it is a bit lower for ovine subjects (0.05–0.5 ε/s) [10]. The switch in strain rate sensitivity would affect loading corrections, as the material may relax more prior to reaching peak loading.

This possibility of strain rate sensitivity is confounded by the small number of donors in this study, where samples were taken from only two animals of a much larger population. The statistical ANOVA that was run for each of the moduli showed there was high inter-animal variability, which would be offset by more samples from more animals. While there is typically high variance in biological samples, high inter-animal variability was observed, as seen in Fig. 4. This may be due to the adipose heterogeneity in local regions of the samples from subject weight loss. All samples were taken from similar regions of the rib cage on each flank, but due to the region specificity of adipose tissue with regards to function and adipose type, high heterogeneity is likely [34]. Regionally in the body and throughout adipose tissue, different ratios of adipocytes, precursor cells, vasculature, immune cells, and nerves are present between individuals, changing material behavior [34]. The tissue tested was white adipose tissue based on the coloring, however, based on the anatomy of typical white adipose tissue, particularly in high energy storing situations, the morphology of the adipocytes and connective tissue is not consistent due to varying levels of hypertrophy or hyperplasia throughout the tissue [34]. With subject weights and weight loss, the morphology was likely even more inconsistent, however, the unique thickness of these samples, which was 1–1.5 inches, was what allowed the indentation tests to be completed by the Hertzian contact assumptions [26][35]. At smaller depths, the contact forces were much smaller, making the signal-to-noise ratio smaller and introducing additional variability into the data. To properly ensure the force measures were high enough to detect, larger depths for the indentation experiment were needed. With these larger depths, thicker samples were required. Since there are few ovine subjects with such a large amount of adipose tissue, the subject pool was particularly small. As a result, this study only had two animal donors, where two samples from each donor were obtained for additional tissue.

Regarding the dynamic experiments, due to the nature of the soft tissue, the surface of the tissue was not perfectly flat, also leading to data limitations. Good contact was ensured while setting up the dynamic tests, but the texture of the tissue surface was of similar magnitude in size to the impactor head, leading to the tests not being completely perpendicular as prescribed on the larger scale. As a result, variations on the impact angle were run in the dynamic simulations. As shown in the simulation set that was run, the angle of impact did affect the resulting force-time curve. The prominent spike in force is diminished with a greater impact angle. It should be noted, however, that when overlaying the spike in the zero-degree case against all the experimental data in Fig. 5 (overlay not shown), the simulated data are still within the range of data collected. Despite this limitation, the simulations showed that the material model, which was based on the spherical indentation tests, did predict the behaviour of the adipose tissue well, particularly when the impact angle was not exactly perpendicular, which we knew to be the case in the experiments. While it could not be independently verified with the experimental data, the force versus time results shown for the model were run with a constant impactor head velocity, thus these data could also be interpreted as force versus displacement if the abscissa values are multiplied by 4 m/s. Looking at the data in this way, the max. depth of penetration of the simulation was 10 mm.

The simulations of the dynamic test did not include failure parameters in the model. It is important to note that dynamic testing did result in tissue failure, as plastic deformation was visible during *ex vivo* experiments. Sun *et al.* reported human adipose tissue failure parameters, including failure stress, but no ovine-specific adipose failure data were available [28]. The addition of failure to the material model would likely decrease the initial spike in force *in silico*. Failure testing of ovine adipose tissue would provide insights that would further improve this model.

Future work should include more animal subjects, as well as high-rate testing (8 m/s or 2000 ε/s) to further analyse loading effects. Clinical imaging, such as MRI and CT, should also be done to determine any macroscopic differences between animal samples to understand the inter-animal variability. Lastly, the resulting validated material model can be input into FE models for dynamic testing. Due to the linear viscoelasticity assumption made, it is suggested for more dynamic FE models, not for quasi-static models.

V. CONCLUSION

This study successfully characterised ovine adipose tissue using spherical indentation, impacted adipose tissue to obtain dynamic force-time data, and validated the adipose material model *in silico* using *MAT_GENERAL_VISCOELASTIC in LS-DYNA. The resulting material model should not be used for quasi-static models due to linear viscoelastic assumptions and is recommended for dynamic applications (>5 ε/s). Given that this ovine tissue model has been characterised and validated, it can be used in detailed whole-body FE models to simulate various environments, such as the NPBI environment, and improve upon the understanding of injury mechanisms.

VI. ACKNOWLEDGEMENTS

The authors would like to thank Dr Graca Almeida-Porada and Wade von Kleeck for their support. This work was supported by the DEVCOM Army Research Lab, which funded this project (#W911NF2120034).

VII. REFERENCES

[1] Cannon, L. (2001) Behind Armour Blunt Trauma - an emerging problem. *Journal of the Royal Army Medical Corps*, **147:** pp. 87–96.
[2] Courtney, M. W. and Courtney, A. C. (2011) Working toward exposure thresholds for blast-induced traumatic brain injury: thoracic and acceleration mechanisms. *Neuroimage*, **54**: pp. S55–S61.
[3] Stuhmiller, J.H. (2008) Blast Injury. *Translating Research into Operational Medicine,* pp. 74.

[4] Yang, Z., Wang, Z., Tang, C., Ying, Y. (1996) Biological effects of weak blast waves and safety limits for internal organ injury in the human body. *Journal of Trauma*, **40**(3 Suppl): pp. S81–S84.
[5] Gibbons, M. M., Dang, X., Adkins, M., Powell, B. and Chan, P. J. J. o. b. e. (2015) Finite element modeling of blast lung injury in sheep. *Journal of Biomechanical Engineering,* **137**(4): p.041002.
[6] Wang, S. C., Bednarski, B., *et al*. (2003) Increased depth of subcutaneous fat is protective against abdominal injuries in motor vehicle collisions. *Annual Proceedings of the Association for the Advancement of Automotive Medicine*, 2003, Lison, Portugal.
[7] Kim, J.-E., Kim, I. H., *et al.* (2014) A computational study of injury severity and pattern sustained by overweight drivers in frontal motor vehicle crashes. *Computer Methods in Biomechanics and Biomedical Engineering*, **17**(9): pp. 965–977.
[8] Comley, K. and Fleck, N. A. (2010) A micromechanical model for the Young's modulus of adipose tissue. *International Journal of Solids and Structures*, **47**(21): pp. 2982–2990.
[9] Machinery, E.-P. Common Viscosity of Liquids. https://www.epakmachinery.com/chart-viscosity-of-common-liquids/. n.d. [Accessed 13 February 2023].
[10] Comley, K. and Fleck, N. (2012) The compressive response of porcine adipose tissue from low to high strain rate. *International Journal of Impact Engineering*, **46**: pp. 1–10.
[11] Sun, Z., Gepner, B. D., *et al.* (2021) Effect of Temperature and Freezing on Human Adipose Tissue Material Properties Characterized by High-Rate Indentation: Puncture Testing. *Journal of Biomechanical Engineering*, **144**(3).
[12] Sun, Z., Lee, S.-H., *et al*. (2021) Comparison of porcine and human adipose tissue loading responses under dynamic compression and shear: A pilot study. *Journal of the Mechanical Behavior of Biomedical Materials*, **113**: 104112.
[13] Sommer, G., Eder, M., *et al*. (2013) Multiaxial mechanical properties and constitutive modeling of human adipose tissue: a basis for preoperative simulations in plastic and reconstructive surgery. *Acta biomaterialia*, **9**(11): pp. 9036–9048.
[14] Miller-Young, J. E., Duncan, N. A. and Baroud, G. (2002) Material properties of the human calcaneal fat pad in compression: experiment and theory. *Journal of Biomechanics*, **35**(12): pp. 1523–1531.
[15] Then, C., Vogl, T., Silber, G. (2012) Method for characterizing viscoelasticity of human gluteal tissue. *Journal of Biomechanics*, **45**(7): pp. 1252–1258.
[16] Calvo-Gallego, J. L., Domínguez, J., Cía, T. G., Ciriza, G. G. and Martínez-Reina, J. (2018) Comparison of different constitutive models to characterize the viscoelastic properties of human abdominal adipose tissue. A pilot study. *Journal of the Mechanical Behavior of Biomedical Materials*, **80**: pp. 293–302.
[17] Hatt, A., Lloyd, R., Bolsterlee, B. and Bilston, L. E. (2023) Strain-dependent shear properties of human adipose tissue in vivo. *Journal of the Mechanical Behavior of Biomedical Materials*, **143**: 105924.
[18] Comley, K. and Fleck, N. (2009) The high strain rate response of adipose tissue. *Proceedings of the IUTAM Symposium on Mechanical Properties of Cellular Materials,* September 17–20 2007, LMT-Cachan, Cachan, France.
[19] Obaid, N., Kortschot, M. T. and Sain, M. (2017) Understanding the Stress Relaxation Behavior of Polymers Reinforced with Short Elastic Fibers. *Materials* (Basel), **10**(5).
[20] Nicolaidis, S. and Arnaud, M. (1998) Physiology of thirst. *Hydration throughout life*, pp. 3-8.
[21] Lau, A., Oyen, M. L., Kent, R. W., Murakami, D., Torigaki, T. J. A. b. (2008) Indentation stiffness of aging human costal cartilage. *Acta biomaterialia,* **4**(1): pp. 97–103.
[22] Mattice, J. M., Lau, A. G., Oyen, M. L., Kent, R. W. (2006) Spherical indentation load-relaxation of soft biological tissues. *Journal of Materials Research*, **21**(8): pp. 2003–2010.
[23] Oyen, M. (2006) Analytical techniques for indentation of viscoelastic materials. *Philosophical Magazine,* **86**(33–35): pp. 5625–5641.
[24] Thomas, P. K., Sullivan, L. K., Dickinson, G. H., Davis, C. M., Lau, A. G. J. C. T. I. (2021) The Effect of Helium Ion Radiation on the Material Properties of Bone. *Calcified Tissue International,* **108**(6): pp. 808–818.
[25] Johnson, K. L. and Johnson, K. L. (1987) *Contact mechanics*. Cambridge University Press: Cambridge, UK.
[26] Lee, E. H. and Radok, J. R. M. (1960) The Contact Problem for Viscoelastic Bodies. *Journal of Applied Mechanics*, **27**(3): pp. 438–444.
[27] Sakai, M. (2002) Time-dependent viscoelastic relation between load and penetration for an axisymmetric indenter. *Philosophical Magazine A: Physics of Condensed Matter, Structure, Defects and Mechanical Properties*, **82**(10): pp. 1841–1849.

[28] Sun, Z., Gepner, B. D., *et al*. (2022) Effect of Temperature and Freezing on Human Adipose Tissue Material Properties Characterized by High-Rate Indentation: Puncture Testing. *Journal of Biomechanical Engineering*, **144**(3).
[29] Silva, M. R., Yuan, Z., *et al*. (2009) Spherical indentation of lungs: Experiments, modeling and sub-surface imaging. *Journal of Materials Research*, **24**(3): pp. 1156–1166.
[30] Lau, A., Oyen, M. L., Kent, R. W., Murakami, D., Torigaki, T. (2008) Indentation stiffness of aging human costal cartilage. *Acta Biomater*, **4**(1): pp. 97–103.
[31] Hartlen, D. C. and Cronin, D. S. (2023) A General Method for Computing an Average Curve and Statistical Response Corridors Using Biomechanical Monotonic and Load-Unload Data.
[32] Alkhouli, N., Mansfield, J., *et al.* (2013) The mechanical properties of human adipose tissues and their relationships to the structure and composition of the extracellular matrix. *American Journal of Physiology-Endocrinology and Metabolism*, **305**(12): pp. E1427–E1435.
[33] Gefen, A., Haberman, E. (2007) Viscoelastic Properties of Ovine Adipose Tissue Covering the Gluteus Muscles. *Journal of Biomechanical Engineering*, **129**: 924-930.
[34] Lynes, M.D., Tseng, Y. (2017) Deciphering adipose tissue heterogeneity. *Annals of the New York Academy of Sciences,* **1411**: 5-20.
[35] Fischer-Cripps, A. (1999) The Hertzian contact surface. *Journal of Materials Science*, **34**(1): pp. 129–137.